

Ultrafast switching to a stable hidden topologically protected quantum state in an electronic crystal.

L. Stojchevska^{1,2}, I. Vaskivskyi¹, T. Mertelj¹, P. Kusar¹,
D. Svetin¹, S. Brazovskii^{4,5} and D. Mihailovic^{1,2,3,*}

¹Dept. of Complex Matter, Jozef Stefan Institute, Jamova 39, Ljubljana, SI-1000, Ljubljana, Slovenia,

²Jozef Stefan International Postgraduate School, Jamova 39, Ljubljana SI-1000, Slovenia

³CENN Nanocenter, Jamova 39, Ljubljana, Slovenia

⁴LPTMS-CNRS, UMR8626, Univ. Paris-Sud, Bat. 100, Orsay, F-91405 France

⁵International Institute of Physics, 59078-400 Natal, Rio Grande do Norte, Brazil

*To whom correspondence should be addressed; E-mail: dragan.mihailovic@ijs.si.

07/04/2014

Hidden states of matter with novel and unusual properties may be created if a system out of equilibrium can be induced to follow a trajectory to a state which is inaccessible or does not even exist under normal equilibrium conditions. Here we report on the discovery of a hidden (H) topologically protected electronic state in a layered dichalcogenide $1T$ -TaS₂ crystal reached as a result of a quench caused by a single 35 fs laser pulse. The properties of the H state are markedly different from any other state of the system: it exhibits a

large drop of electrical resistance, strongly modified single particle and collective mode spectra and a marked change of optical reflectivity. Particularly important and unusual, the H state is stable for an arbitrarily long time until a laser pulse, electrical current or thermal erase procedure is applied, causing it to revert to the thermodynamic ground state. Major observed events can be reproduced by a kinetic model describing the conversion of photo excited electrons and holes into an electronically ordered crystal, thus taking into account a dynamic conversion of particles among reservoirs of liquids of electrons and holes, and of an electronically ordered crystal. converting a Mott insulator to a conducting H state. Its long-time stability follows from the topological protection of the number of periods in the electronic crystal.

Extreme conditions necessary for reaching hidden many body states can be created in the laboratory using laser photoexcitation in condensed matter systems. Typically, the ground state ordering can be temporarily destroyed, but on cooling the system reverts back in a few picoseconds, exceptionally passing through a transient metastable state. So far, a few such metastable states have been shown to persist on timescales between 10^{-9} - 10^{-3} s (1,2,3,4,5,6,7) before recovering to the ground state by a combination of thermal, electronic and lattice relaxation processes (2). Stability of photoinduced states has been demonstrated in a manganite (6) and in chalcogenide glasses (8), where switching occurs between neighbouring thermodynamic states, but no hidden states are involved in these cases.

In this paper, we report for the first time on bistable switching to a hidden (H), spontaneously ordered macroscopic quantum state whose properties are distinct from any other state in the equilibrium phase diagram. The hidden state transition (HST) occurs in a layered quasi-2D chalcogenide $1T$ -TaS₂ crystal, a system which exhibits multiple competing ground states already under equilibrium conditions. Some of the states are shown schematically in Fig. 1A.

Near $T_{c0} = 550$ K $1T$ -TaS₂ forms an incommensurate charge-density-wave (IC) with an associated lattice distortion. On cooling these modulations sharpen to form star-shaped polaron clusters (Fig.1 A). Their ordering is thought to be responsible for a variety of phases, causing a transition to a nearly commensurate (NC) state for $T < T_{c1} = 350$ K, and a hysteretic first-order transition to a gapped commensurate (C) phase at $T_{c2} \simeq 183$ K. On heating, the system develops a triclinic stripe-like ordered state around 223 K which reverts to the NC state at $T_{c2} \simeq 283$ K (9). Further nearby equilibrium states are revealed upon the application of external pressure (10) or doping (11), both of which make $1T$ -TaS₂ superconducting.

To induce the HST, we use a single sub-35 fs Write (W) pulse from an amplified Ti-Sapphire laser at 800 nm with energy $U_W \simeq 1$ mJ/cm². After inducing a HST at 1.5 K, the 4-probe resistance $r(T)$ drops approximately 3 orders of magnitude and *remains in this state indefinitely* at this temperature (Fig. 1B). Upon heating, $r(T)$ is approximately constant up to 60 K, whereupon it increases and merges to the virgin $r(T)$ curve corresponding to the C state above $T_H \sim 100$ K. The I - V characteristic remains linear throughout. Empirically we found that the H state can be *completely* erased (E) by a pulse train of 10^4 50 ps pulses, each with $U_E \simeq 1$ mJ/cm². Alternatively, Joule heating can be used for erasure by passing a ~ 0.1 mA current through the device. In all three cases the system reverts to the C state. Stable switching can be achieved also at intermediate temperatures up to $T \sim 70$ K. The effect is entirely reversible from cycle to cycle, sample to sample, irrespective of the sample growth batch, and there appears to be no limit on the number of W/E cycles that can be performed. (Experimental details on thermal protocols, including ageing effects (12), and a description of the laser lithography used to manufacture the contacts are given in the supplementary material (SM)).

To gain insight into the microscopic nature of the hidden state, we investigate the single-particle and collective excitations, using Pump-probe (P - p) spectroscopy with the P and p pulse energies kept low ($< 10\mu\text{J}/\text{cm}^2$ and $< 1\mu\text{J}/\text{cm}^2$ respectively) to ensure minimal disturbance of

either state. The sample reflectivity $R(t)$ is simultaneously recorded by the probe (p) beam. In Fig. 2 A to D we first present the transient reflectivity $\Delta R/R$ of $1T$ -TaS₂. In the virgin C state we observe oscillations due to the coherent excitation of the amplitude mode (AM) and phonons which are superimposed on a background from exponentially decaying single particle (SP) excitations across the gap ($I3$). The spectrum $S(\omega)$ obtained by Fourier transformation shows a strong amplitude mode at 2.46 THz, and weaker phonon modes at 2.1, 2.18, 3.2 and 3.85 THz (see Fig.2B). The HST modifies the $\Delta R/R$ (Fig. 2B) and the SP signal is reduced significantly. In the spectrum after the HST shown in Fig.2B the AM peak at 2.46 THz *disappears*, in favour of a new mode at 2.39 THz; intensities of modes at 3.10 THz and 3.85 THz are reduced, and some additional spectral intensity appears between 2 and 2.5 THz. On heating, the spectrum of the H state remains unchanged until ~ 70 K. Above 70 K it gradually reverts back to the C state. Concurrent with the switching of the AM and phonons, we observe a switching of reflectivity R at 800 nm, as shown in Fig. 2 D. All the observations display typical threshold behaviour as a function of U_W : below threshold fluence the resistivity, AM frequency and reflectivity revert to the C state values after the W pulse. Close to threshold fluence, the AM shows bimodal behaviour, which we interpret as incomplete switching. Importantly, no intermediate shift of the AM is observed, indicating distinct two-phase behaviour. The H state spectrum is quite different from the NC state spectrum (Fig. 2 A and B) or the T state spectrum (see SB), indicating that it is not related to the equilibrium states.

We emphasize some remarkable features of the HST: **1.** After photo-excitation the H state spontaneously orders below T_H , as indicated by the narrowness of the AM peak and the fact that *no partial frequency shift* is ever observed even when incomplete switching is caused by near-threshold excitation (see SM). **2.** The switching occurs *only with short pulses*, and the threshold increases with increasing τ_W as shown in Fig. 2 C and - remarkably - can no longer be achieved with $\tau > 4$ ps at any U_W . **3.** The H state is completely stable until erased, or heated

above ~ 70 K. Note that T_H has no special significance under equilibrium conditions and is relevant only for describing the transition from the H state to the C state.

To understand these unusual phenomena, we first introduce a scenario for switching based on the current understanding of the electronic ordering in $1T$ -TaS₂ (9,14,15,16), and then describe the results of a minimal phenomenological model which offers insight into how transient photodoping can lead to a stable ordered state.

The relevant electronic states of $1T$ -TaS₂ in the C state which are within reach of our 1.5 eV laser photons are shown in Fig. 3 C. They are formed predominantly from a single Ta d band which is split into subbands by the formation of a CDW depicted in Fig 1 A. Six of these subbands are filled with 12 electrons per new large unit cell forming a manifold of occupied states up to 0.4 eV below E_F (shown in blue in Fig. 3 C). The 13th left-over electron is localised on the central Ta causing inward radial displacements of 12 neighbours in the shape of a star of David (14,15), thus forming a self-localized polaron. The 13th electron gives rise to a half-filled narrow metallic band straddling the Fermi level; but this band is further split by the Coulomb interaction into two Hubbard bands (plotted green in Fig. 3 C) (15), whereby the upper one merges with the manifold of unoccupied subbands above E_F , while the lower one is ~ 0.2 eV below E_F - still well above the top of the valence band at -0.4 eV, which makes the C state a Mott insulator in the form of a polaronic crystal (10,14,15). In the photoexcited case however, a charge imbalance can cause voids in the polaron lattice which - upon relaxation - leads to the formation of a spontaneously ordered H state. The possibility of both positive and negative discommensurations has been indicated by STM experiments (9), indicating that the system can accommodate both extra holes or extra electrons.

Recent experiments show that the Mott gap rapidly melts within ~ 50 fs after photo-excitation (17), but after $0.5 \sim 1$ ps, the AM oscillations are visible again, indicating the recovery of the C state within a few AM cycles. Since the e - h energy relaxation occurs on

a similar timescale ($\tau_E \sim 1$ ps) (13,17), the condensation into the crystalline state competes with $e - h$ recombination.

Photoexcitation initially creates equal numbers of electrons (e) and holes (h) by an inter-band transition, followed by rapid intraband thermalisation via scattering amongst themselves and with the lattice, as well as transitions between different bands, reaching states near the Fermi level and melting the C order on a timescale on the order of 50 fs (17,18,19,20). The maximum effective electronic temperature reached in the process is $T_e \sim 1000$ K, while the lattice reaches ~ 150 K within 3 – 5 ps, whereupon the two are in quasi-equilibrium. (See SM for temperature measurements and model estimates). However, the large asymmetry of the band structure in this compound (14), can also lead to a photodoping effect: the e and h scatter and lose energy at different rates, leading, on the sub-5-picosecond timescale, to a transient imbalance of their respective populations n_e and n_h .

Let's now examine the photodoping effect in more detail. Doping away from half-filling of a conventional Mott-Hubbard state on a rigid lattice leads to a conducting state. But here photo-doping disturbs the polaronic deformations. Let's consider the effect of a photo-doped hole, which annihilates with the localised 13th electron. The annihilation removes the charge at the centre of the polaron, rapidly dissolving the polaronic distortion and leaving a void in its place. In the standard polaron picture (21), its dissolution releases a band state from which the polaron was originally formed, which makes the system conducting. Since some of the 13th electrons have been annihilated by holes, not all ions in these regions are charge compensated, and they have an excess charge. Yet these regions cannot conduct because the remaining 12 electrons are in filled states within the gap formed by the long-range CDW (see Fig. 3 C). The excess charge within these regions will be screened by the electrons which are now transferred to the delocalised bands. At a sufficiently low T and high concentration n_v , these voids are expected to aggregate by diffusion into domain walls. The overall state becomes conducting

via the band states released by the annihilated polarons which, if ordered, would form a new incommensurate structure. We can also imagine that photo-excited electrons could squeeze into the structure in between the polarons creating interstitials with a concentration n_i (9). Together with voids with a concentration n_v the total "intrinsic defect" concentration $n_d = n_v - n_i$ may have either sign. Overall charge conservation $n_h + n_v = n_e + n_i$ gives the imbalance of the current carriers $n_d = n_e - n_h$. Conventionally, photodoping is a transient effect, so once $e - h$ symmetry is recovered, the voids and domain walls disappear and the C state is restored. However, if the voids can be stabilised by collectively ordering into a long-range ordered state, the final state is different than the original one.

Overall charge conservation requires that the concentration n_v of the voids or their walls compensates for the imbalance $n_e \neq n_h$ of electron and hole concentrations in delocalized bands, arresting their mutual recombination and maintaining a metallic state. In either case, local strain causes subsequent self-reorganisation of these voids (or extra electrons), giving rise to a long-range ordered structure with an excess of charge carriers with respect to the C state.

Now we outline a plausible minimal model for the metastable state, which may have phenomenological implications beyond our detailed speculations on the nature of microscopic processes in this particular material. The model details, the calculation and more results are presented in the Appendix.

The free energy $F_d(n_d)$ appropriate for the formation of the charge-ordered state outlined above (16) needs to include the effect of repulsion between the domain walls, their crossings (16,22,23), and should reproduce the first order nature of the transition (16,23). The $F_d(n_d)$ based on these considerations and existing models (16,23) is plotted in Fig. 3 B.

To obtain the time dependencies of concentrations $n_e(t)$, $n_h(t)$ and of the electronic temperature $T(t)$ we consider the recombination rates of e and h across the spectral gap and into the new ordered state. Apart from the densities, the rates depend on the separate chemical poten-

tials $\mu_i(t) = \partial F_i / \partial n_i$ for the electrons, holes and defects (we assume that the sub-systems are more or less equilibrated internally (19)). The difference in chemical potentials gives the energy released when particles are exchanged among the reservoirs which determines the temperature evolution. In equilibrium, the μ_i for all the three reservoirs must be equal, so the intersection of the three surfaces μ_e , μ_h and μ_d , as functions of n_e and n_h and subject to the constraint $n_d = n_h - n_e$ gives the thermodynamically stable end points of the system. These are shown in Fig. 3 D, plotted for an arbitrary intermediate temperature $0 < T < T_H$. The condition $\mu_h = \mu_d = -\mu_e$ gives two stable points, which correspond to the free energy minima shown in Fig. 3 B: point C where $n_e = n_h$, and point H , where $n_e - n_h = n_d \neq 0$. The third intersection U is unstable since it corresponds to a maximum of the free energy.

The relaxation processes between the charge reservoirs considered by the model are shown schematically in Fig. 3 C (See the Appendix for more details). In Figs. 4 A - C we show the calculated trajectories of $n_e(t)$ and $n_h(t)$ after a laser pulse excitation plotted as a function of time t in the form of parametric plots for different cycles. The plots include the lines of intersections between the pairs of chemical potential surfaces from Fig.3 D, indicating the possible end points (H or C) corresponding to the temperature at the end of the cycle. In the W cycle, we start in the C state at low T where $n_e = n_h \simeq 0$ (point O). For excitation above threshold $U_W > U_T$ (Fig. 4 A), the laser pulse causes the electronic temperature to increase and the system trajectory initially follows the C state line (where $n_e = n_h$), then makes a loop and ends at point H (where $n_d \neq 0$). In this cycle, the system trajectory goes around the energy maximum point U behind which the H point is hidden.

Below threshold ($U_W < U_T$), the system initially follows the same path, but the final temperature reached by the system is too low for there to be an intersection of all three chemical potentials, so the system returns back to state C (Fig. 4 B). The appearance of a switching threshold observed in the experiments is thus described by the model. In the E cycle we start

from the hidden state at point H (Fig. 4 C). Increasing T above a critical value causes the system to follow curve **1** towards the commensurate state C' at an elevated temperature $T > T_H$. Cooling thereafter causes it to return via **2** to the stable point C , reproducing the cycle performed in our experiments.

We can now also understand why switching does not occur for $\tau > 4$ ps: Electron-hole asymmetry may be present as long as the entire electronic system is out of equilibrium with the lattice (up to $3 \sim 5$ ps). With pulses longer than a critical length which is related to the electron/hole energy relaxation time, the H state can no longer form. Changing the W pulse length τ within our model and plotting the threshold U_T as a function of pulse length τ , we obtain the curve shown in Fig. 2 C. The model closely follows the observed behaviour, whereby no stable H point is reachable for pulses longer than a critical value τ_c , observed experimentally at ~ 4 ps.

The main nontrivial observations, namely the appearance of a switching threshold for the W pulse fluence, its critical pulse-length dependence, the threshold temperature for the E cycle, and the high conductance can thus be reproduced. Moreover, the narrow AM spectrum is a direct consequence of the predicted homogeneous long range order in the H state. The observation of a mid-gap spectral feature following sub-threshold photoexcitation as reported recently(19,24,25) is consistent with a transient change of polaron density.

The reason for the remarkable stability of the H state over an arbitrarily long time is that it is topologically protected: The domain wall density n_d cannot change continuously, but can do so only in discrete steps, only when the number of periods of the electronic crystal changes, which is quantized. Such an effect as has been demonstrated in 1D CDWs (26,27). This constraint - and its energetically costly resolution by proliferation of topological plane and line defects - resembles the protection and inhibited decay of super-currents in superfluids and superconductors where the intrinsic defects are phase slips and vortices. Here, on a microscopic level,

proliferation of new domain walls provides a mechanism for spectral flow of particles across the spectral gaps which converts polaronic states to/from band states. The creation and motion of such extended objects will be substantially slowed down by the presence of intersecting discommensurations and finally arrested by pinning to lattice defects. The E cycle may be explained by the creep of extended defects which is known to be promoted by heating above an irreversibility line characteristic of pinning phenomena.

Previous time-resolved experiments in $1T\text{-TaS}_2$ failed to detect switching because they were performed either with insufficient fluence(18), or the ambient temperature was too high(20). The mechanism for the creation of a topologically protected state by a nonequilibrium quench is generic and is likely to be found in other charge-ordered materials with multiple electronic reservoirs. The switching is caused by relatively weak and short pulses, which - considering the large change in resistance and optical reflectivity - has obvious application potential. The effect also opens the way to the search for new generations of room temperature non-volatile memory elements in electronically ordered materials. As a memory element, switchable by sub-35 fs pulses, our device is already comparable to, or exceeds the current speed record of 40 fs in magnetic materials (28).

1 Appendix: the calculation of the system trajectory

The theory was developed on a basis of a phenomenological approach which leads to a minimal and computationally treatable model, and which is compatible with existing microscopic pictures. Our model is independent of underlying microscopic details and can be only complicated further, but this was not necessary as shown by the successful numerical solutions of the equations below.

The focus is upon three reservoirs of electrons: electrons and holes as mobile charge carriers with concentrations n_e and n_h and the crystallized electrons with the concentration $1 - n_d$ where

$n_d = n_v - n_i$ is the relative density of intrinsic defects (interstitials "i" and voids "v" as explained above; both are known to be present (9). Altogether, the concentrations are subject to the charge conservation law $n_e - n_h = n_v - n_i = n_d$. The crystalline density, hence the concentration of its defects, can be changed only by proliferation of topological defects, akin to vortices in superfluids, which is allowed at high T of initial dynamics but is arrested at low T of the already formed H state.

The total free energy, which we shall consider additive, $F(n_d, n_e, n_h) \approx F_d(n_d) + F(n_e) + F(n_h)$ determines the partial chemical potentials $\mu_j = \partial F / \partial n_j \approx \mu_j(n_j)$ (these are also functions of the temperature) of the reservoirs which must be all equilibrated in the static regime. The electrons and the holes from the nominally empty and filled band states will be considered as particles with 2D spectra $\epsilon_{e,h}(p) = \Delta_{e,h} + p^2/2m_{e,h}$ characterized by their activation energies - the gaps $\Delta_{e,h}$ and by effective masses $m_{e,h}$ giving constant densities of states $N_{e,h} \sim m_{e,h}$ above the respective gaps. That yields the chemical potentials as

$$\mu_{e,h}(n) = \Delta_{e,h} + k_B T \ln(\exp(n_{e,h}/(k_B T N_{e,h}) - 1). \quad (1)$$

The necessary free energy $F_d(n_d)$ of the crystalline reservoir can be taken just to satisfy the fact of the first order phase transition in equilibrium between the *C* and *IC* phases, which is the experimental fact as well as the results of thermodynamical calculations. We went a bit further to justify the chosen form of F_d by referring to a general theory (23) of weakly incommensurate triangular lattices. Assuming the symmetry between vacancies and interstitials, i.e. with respect to the sign of n_d , we choose the parametrization

$$F_d(n_d) = E_{DW}(C_0|n_d| + C_1|n_d|e^{-1/(\xi|n_d|)} - C_2\xi n_d^2 + C_4\xi^3 n_d^4) \quad (2)$$

where C_n are numeric constants. Here ξ is the domain wall width, E_{DW} is its energy scale per a constituent defect. The first two terms are standard for a picture of the 2nd order *C-IC*

transition: in thermodynamic equilibrium, the coefficient $C_0 < 1$, as a function of T , reduces the DW energy and for $C_0 < 0$ the walls start to be created but their concentration is stabilized by the repulsion given by the second term $\sim C_1$. The next term $\sim C_2$ appears for non-collinear arrays of domain walls which now intersect in points with a concentration $\sim n_d^2$. A key point (23) is that this energy is expected to be negative, which we took into account with the sign “-” of the term $\sim C_2$ in (2). Together with the last stabilizing term $\sim C_4$ to take into account the repulsion between the crossings, we obtain the desired non-monotonous curve for F_d shown in Fig. 3A. The chemical potential of the crystalline reservoir is then:

$$\mu_d(n_d) = E_{DW}(C_0 + C_1(1 + \frac{1}{\xi|n_d|})e^{-1/(\xi|n_d|)} - 2C_2\xi|n_d| + 4C_4(\xi|n_d|)^3)\text{sign}(n_d). \quad (3)$$

The three surfaces of chemical potentials $-\mu_e$, μ_h and μ_d as a function of n_e , n_h and $n_d = n_e - n_h$ respectively are shown in Fig. 3B. (μ_h and μ_d , as both counting the electron’s deficiencies, should be always taken with an opposite sign with respect to μ_e .)

Mutual transformations among the reservoirs, together with the concomitant heat production, are dictated by imbalances of three partial chemical potentials μ_j . The corresponding kinetic equations are chosen in a simplest form satisfying to the condition that the exchange rate among any two reservoirs vanishes when the corresponding chemical potentials become equal $\delta\mu_{i,j} = 0$. To model the nonequilibrium evolution, we need to consider the relaxation kinetics between the three reservoirs.

The rates R_{ij} of particles’ exchange among the reservoirs may be complicated functions of n_j , μ_j , and T and we need to make physically motivated assumptions. It is common, from physics of semiconductors to gapful correlated systems, to take the bi-particle form of the e-h recombination $R_{eh} \sim n_en_h$. The linear relations $R_{hd} \sim n_h$ and $R_{ed} \sim n_e$ imply that the band particles can transform themselves into defects without meeting another particle, e.g. the holes

can annihilate with a main part of polarons rather neglecting the small concentration of defects. In principle the bi-modal parts $R_{ed}^{bm} \sim n_e n_d$ and $R_{hd}^{bm} \sim n_e n_d$ can be also present which we shall not consider here keeping the minimalistic approach. Next we use the most general principle that, as functions of potentials mismatches, R_{ij} changes the sign passing through zero when the potentials coincide: $\delta\mu_{i,j} = 0$. Again, we take it into account in a simplest form of the linear dependence $R_{ij} \sim \delta\mu_{i,j}$. Finally, kinetic equations for the time evolution of $n_h(t)$ and $n_e(t)$ acquire the form:

$$\frac{dn_h}{dt} = -k_{eh}n_en_h(\mu_e + \mu_h) - k_{hd}n_h(\mu_h - \mu_d) + P(t) \quad (4)$$

$$\frac{dn_e}{dt} = -k_{eh}n_en_h(\mu_e + \mu_h) - k_{ed}n_e(\mu_e + \mu_d) + P(t) \quad (5)$$

where k_{ij} are the coefficients of the recombination rates $R_{i,j}$ after extracting dependencies on $n_{i,j}$ and $\delta\mu_{i,j}$, $P(t)$ is the temporal profile of particles production. As a justification, notice a distant resemblance of these equations with basic ones describing the photo-voltaic devices (see e.g. (29,30); superficially, n_d can be compared with a part of electrons trapped by impurities or lattice defects.

The temperature evolution is taken into account by the energy balance equation

$$J = C_T dT/dt = \sum_j \mu_j (dn_j/dt), \quad (6)$$

where C_T is the heat capacity. The formulas (4,5) and (6) form a complete set of equations governing the system evolution. Their solution yields the trajectory of the Fig. 3, and the partial time dependencies in Fig. 5.

In these equations, the time is in ps and k_{ij} are in ps^{-1} , the laser pulse length is $\tau = 0.035$ ps. Other quantities are dimensionless: n_j as concentrations per enlarged unit cell of one star; the energies as given in units of the electrons' gap Δ_e . The parameters used for calculation

presented in the main text and in Fig. 5 below are as follows. The hole gap is taken as $\Delta_h = 1.4$ (following a prevailing information from experiments and band calculations that the Fermi level is closer to the upper rim of the gap), and the densities of states are $N_h = 1.2$, $N_e = 1$. For electrons there may be an uncertainty because we do not know for sure if they thermalize to the bottom of the conduction band or to the upper Hubbard level which positions look to be close, see (31) and refs. therein. Also the electronic states are not accessible to photo-emission experiments. Still, it is known from STS (32) and optics (33) that the total gap is $\Delta_e + \Delta_h = 0.6\text{eV}$, so our energy unit is 0.25eV .

Parameters in Eqs. (2,3) are adjusted such that the free energy F_d shows the appropriate minimum as shown in Fig. 3A: $C_0 = 0.22$, $C_1 = 1$, $C_2 = 1$ and $C_4 = 2$. The domain wall size is $\xi = 3$, in lattice units, and the domain wall energy scale is $E_{DW} = 2$. So the energy to initiate one defect is taken as $E_d = C_0 E_{DW} = 0.44\Delta_e = 0.11\text{eV}$. $k_{eh} = 20\text{ ps}^{-1}$, $k_{hd} = 20\text{ ps}^{-1}$ and $k_{ed} = 10\text{ ps}^{-1}$; their magnitudes are estimated from the observed single particle relaxation rate in Fig. 2B. The trajectory is very robust with respect to parameters k_{ij} , changing their magnitude by a factor of 2 has a minor effect on the plots, provided that $k_{hd}/k_{ed} > 2$. For these parameters, the threshold laser pulse energy for switching to the H state is $U_T = 0.8$.

The temporal evolution of n_e , n_h , n_d and T is plotted in Fig. 5 above and below U_T , corresponding to the trajectories shown in Fig. 3. Notice that the temperature saturates quite fast while the evolution of concentrations keeps a longer time towards H state and much longer time towards the C state.

We acknowledge discussions with L. Forro, V. V. Kabanov, N. Kirova, P. Monceau, E. Tossatti and E. Tutis. Samples were grown by P. Sutar and H. Berger. We also acknowledge funding from ARRS, European restructuring funds (CENN Nanocenter) and the ERC advanced grant TRAJECTORY.

1. S. Koshihara, et al., *Phys. Rev. B* **42**, 6853 (1990).

2. K. Nasu, *Photoinduced phase transitions*, (World Scientific, 2004).
3. H. Okamoto et al., *Phys. Rev. B* **70**, 165202 (2004).
4. A. Cavalleri, et al., *Phys. Rev. Lett.* **87**, 237401 (2001).
5. S. Tomimoto, S. Miyasaka & T. Ogasawara, *Phys Rev B* **68**, 035106 (2003).
6. N. Takubo et al. *Phys. Rev. Lett.* **95**, 017404 (2005); K. Nasu, H. Ping and H. Mizouchi, *J. Phys.: Condens. Matter* **13**, R693 (2001).
7. G. Yu, et al., *Phys. Rev. Lett.* **67**, 2581 (1991); D. Fausti, et al., *Science* **331**, 189 (2011).
8. A. Zakery and S.R. Elliott, *Optical nonlinearities in chalcogenide glasses and their applications.*, New York: Springer (2007).
9. R. Thomson, B. Burk, A. Zettl, and J. Clarke, *Phys Rev B* **49**, 16899–16916 (1994).
10. B. Sipos, et al., *Nat. Mater.* **7**, 960 (2008).
11. L.J. Li, et al. *Eur. Phys. Lett.* **97**, 67005 (2012).
12. T. Ishiguro and H. Sato, *Phys. Rev. B.* **44**, 2046 (1991)
13. J. Demsar, L. Forro, H. Berger, & D. Mihailovic, *Phys Rev B* **66**, 041101 (2002).
14. K. Rossnagel & N. Smith, *Phys. Rev. B* **73**, 073106 (2006) and references therein.
15. E. Tosatti and P. Fazekas, *J. Phys. Colloques* **37**, C4 (1976).
16. K. Nakanishi and H. Shiba, *J. Phys. Soc. Jpn.* **43**, 1839 (1977).
17. J.C. Petersen et al., *Phys.Rev.Lett.* **107**, 177401 (2011)
18. S. Hellmann et al., *Phys. Rev.Lett.* **105**, 187401 (2010).

19. L. Perfetti, et al. *New J. Phys.* **10**, 053019 (2008).
20. M. Eichberger et al, *Nature* **468**, 799 (2010).
21. F. Clerc et al., *J. Phys.: Condens. Matter* **19**, 255002 (2007).
22. W. McMillan, *Phys Rev B* **14**, 14961502 (1976).
23. For a review and refs. see P. Bak, *Rep. Prog. Phys.* **45**, 597 (1982).
24. N. Dean, et al. *Phys. Rev. Lett.* **106**, 016401 (2011).
25. K. Ishizaka et al., *Phys.Rev.B* **83**, 081104(R) (2011)
26. D.V. Borodin, et al, *JETP* **66**, 793 (1987) and refs. therein;
27. S.G. Zybtsev, et al, *Nat. Comms.* **1**, 85 (2010).
28. A. Kirilyuk, A. Kimel, & T. Rasing, *Rev. Mod. Phys.* **82**, 2731 (2010).
29. J. Piprek, *Semiconductor Optoelectronic devices* (Academic Press, SanDiego, 2003).
30. S. Selberherr, *Analysis and Simulation of Semiconductor Devices*, Springer-Verlag, Vienna, Austria, 1984.
31. J.K. Freericks¹, H.R. Krishnamurthy, Yizhi Ge, A.Y. Liu & Th. Pruschke, *Phys. Status Solidi B* **246**, 948954 (2009).
32. Ju-Jin Kim, W. Yamaguchi, T. Hasegawa & K. Kitazawa, *Phys. Rev. Lett.* **73**, 2103 (1994).
33. L. V. Gasparov and K. G. Brown, A.C. Wint, D.B. Tanner, H. Berger, G. Margaritondo, R. Gaal, and L. Forro, *Phys. Rev. B* **66**, 094301 (2002).

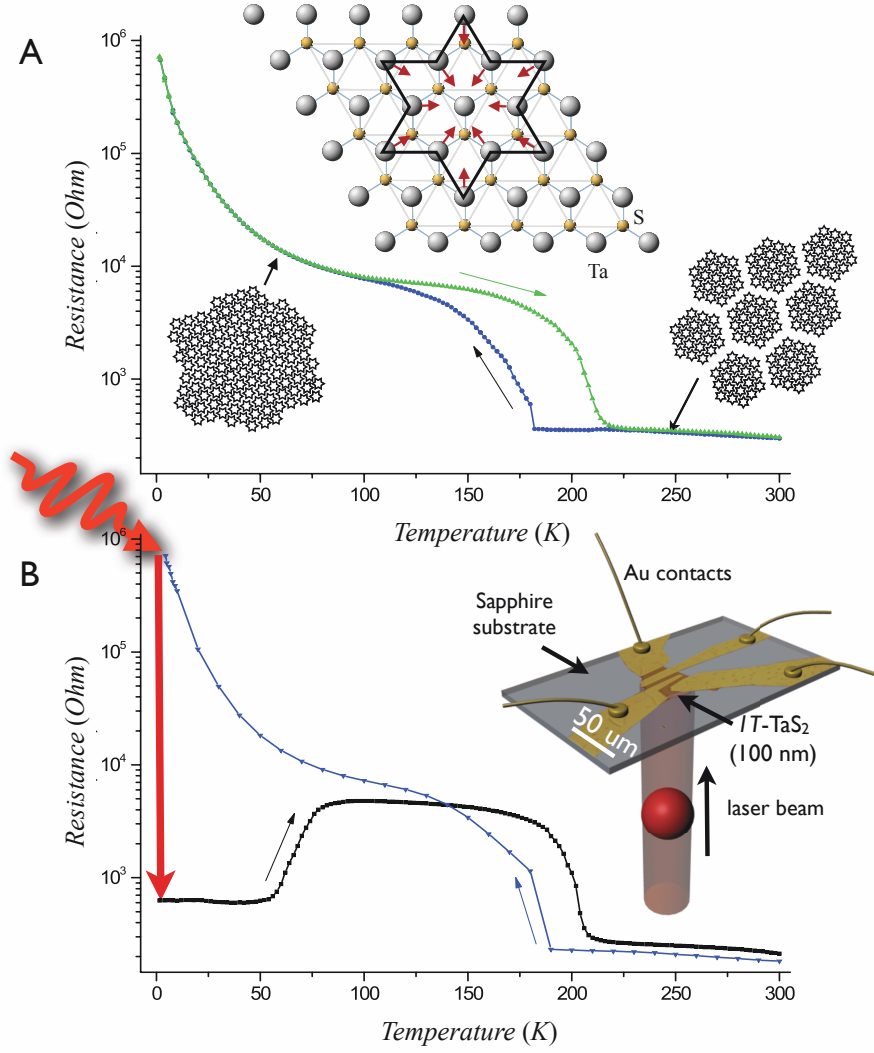


Figure 1: **Fig. 1.** Resistivity switching of 1T-TaS₂ by a 35 fs laser pulse at 800 nm. (A) The T -dependence of the 4-probe resistance $r(T)$ on temperature cycling. The inserts show schematically the lattice distortions associated with an individual polaron and their ordering in the NC and C states respectively. (B) The drop of r at 1.5 K after a single pulse with $U_w > U_T$ (red arrow). On heating the resistance reverts back between 60 and 100K (black curve). The insert shows a schematic of the sample and contacts, which are from an optical microscope image.

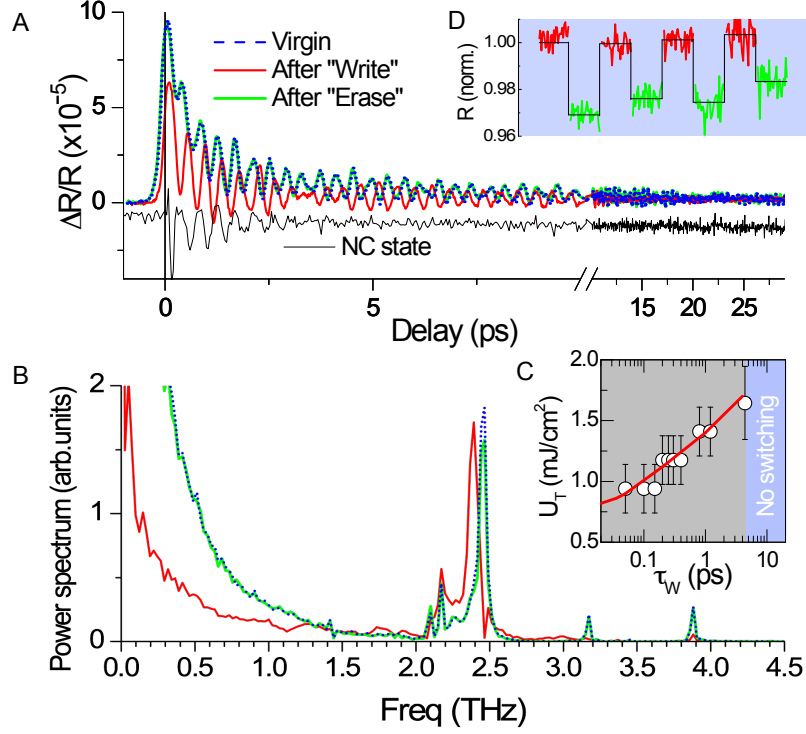


Figure 2: Fig. 2. (A) The transient reflectivity $\Delta R(t)/R$ of $1T$ -TaS₂ in the virgin state (blue dashed line), after exposure to a 50 fs W pulse (red line), and after an E pulse (green line). For comparison, the thin black line is the data in the *NC* state at 220 K recorded on cooling (the trace is offset for clarity). (B) The corresponding FT spectra $S(\omega)$ using the same color notation. Note the complete disappearance of the AM at 2.46 THz in the *H* state, and clean switching back after the E pulse. The switching is also observed for the modes at 2.3, 3.2 and 3.85 THz. The *NC* state spectrum, as well as the *T*-state spectrum recorded at 240 K on heating (not shown) are qualitatively different than either the *C* or *H* state spectra. (C) The switching threshold fluence U_T as a function of pulse length τ_W measured optically with the Pump-probe experiments. The red line is predicted by the model calculation. (D) The reflectivity at 800 nm recorded with the photodiode during a sequence of alternating W and E pulses. (The noise is from the laser.)

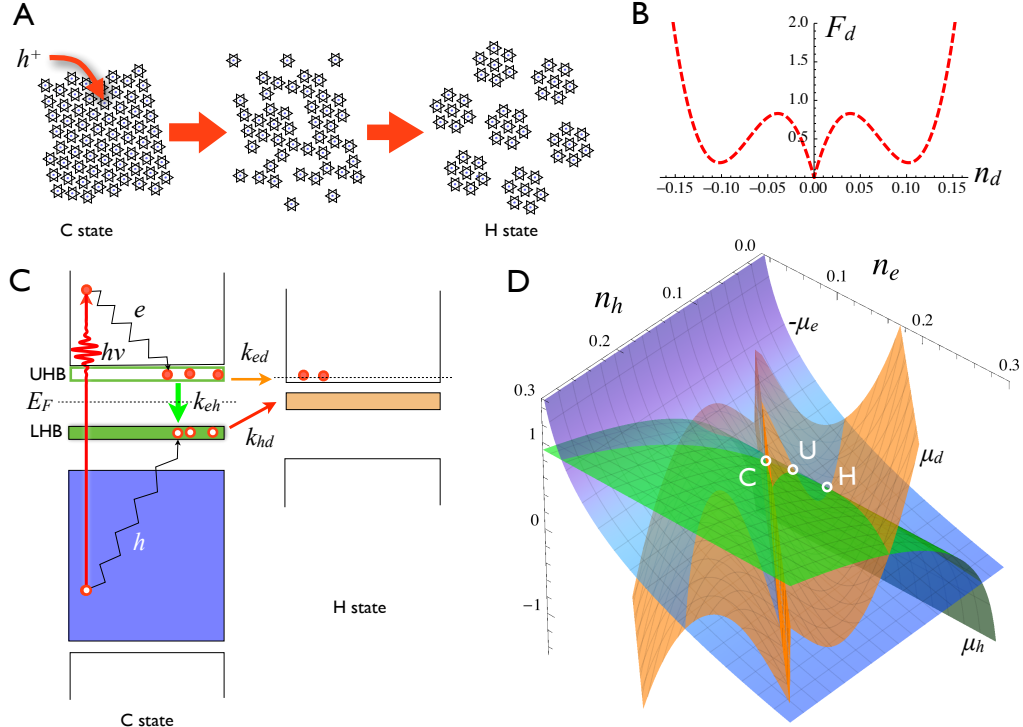


Figure 3: **Fig. 3.** (A) A schematic diagram of the reordering following a laser pulse. First a hole annihilates with a polaron, causing voids in the structure, which reorganise into a long-range ordered structure with a wavevector shift δq is related to the number of defects by charge conservation $\delta q/\pi \simeq n_d$. Loosely, the structure may be thought of as polaron clusters separated by domain walls. (B) The CDW free energy F_d (dashed red line) as a function of n_d . (C) A schematic energy levels diagram of the C state based on refs. (14,15,28). Occupied bands in blue are those from Ta atoms within each polaron in Fig. 1. The Hubbard bands are shown in green. Photoexcitation, initial energy relaxation and subsequent relaxation processes of the e and h amongst themselves and to a new incommensurate H state are shown schematically. (D) The chemical potential surfaces $-\mu_e$ (blue), μ_h (green) and μ_d (orange) respectively as a function of n_e and n_h . The intersections C and H are commensurate and incommensurate stable points of the system respectively.

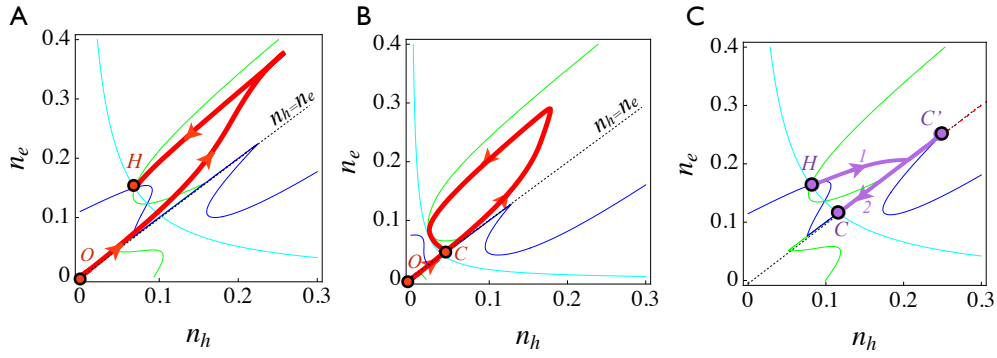


Figure 4: **Fig. 4.** (A) The system trajectory system (thick red line) above switching threshold $U_W > U_T$ on a parametric plot of $n_e(t)$ and $n_h(t)$ as a function of time superimposed on lines of partial equilibria given by the intersections $\mu_e = -\mu_d$ (green), $\mu_h = \mu_d$ (blue) and $\mu_e = -\mu_h$ (cyan) drawn for the final temperature after the system has stabilized. (B) Same as (A) except below threshold $U_W < U_T$. The system now returns to the C state. (C) Model trajectory of erasure by heating in the H -state (purple line): the trajectory first leaves the H -point, then joins the commensurate line. After reaching a maximum at C' , on cooling the system returns to point C .

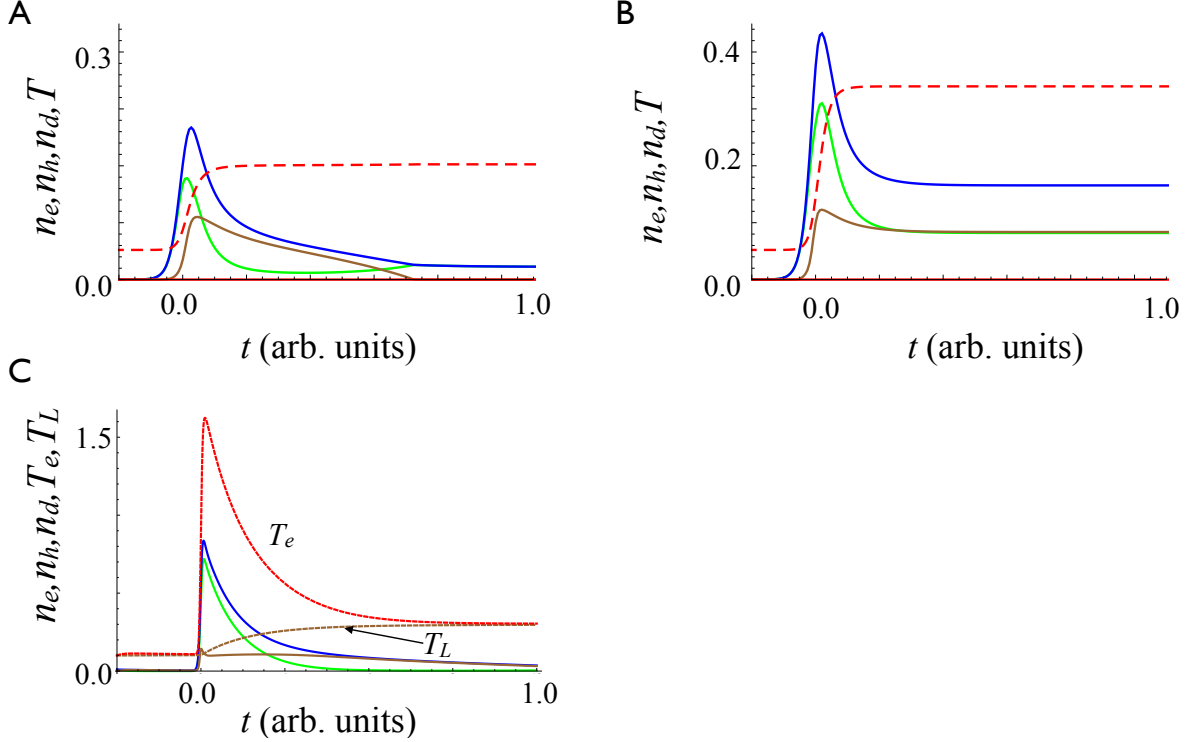


Figure 5: The calculated n_e (blue), n_h (green), n_d (brown) and the temperature T (red dashed) as functions of time using the equations (4,5) and (6): a) below threshold ($U_W < U_T$) and b) above threshold ($U_W > U_T$). The initial temperature was taken as $T = 0.1\Delta_e/k_B$. The corresponding parametric plots of n_e and n_h are shown in Figs. 3 D and E respectively. Note that the calculation does not discuss the cooling part of the cycle, so the temperature remains high after all the pulse energy is transferred. In C we show the results of a calculation which includes the two-temperature model for $U_W > U_T$. n_e (blue), n_h (green), n_d (brown) are qualitatively similar to the results of the simple model calculation (B). The electronic and lattice temperatures T_e and T_L are shown by the red-dashed and brown-dashed lines respectively.